Case Studies in Thermal Engineering 26 (2021) 101042

Contents lists available at ScienceDirect

Case Studies in Thermal Engineering

journal homepage: www.elsevier.com/locate/csite

Numerical investigation of unsteady flow across tandem square cylinders near a moving wall at $Re = 100$

Rajendra S. Rajpoot [a], K. Anirudh [a,b], S. Dhinakaran [a,*]

[a] The Centre for Fluid Dynamics, Department of Mechanical Engineering, Indian Institute of Technology Indore, Khandwa Road, Simrol, Indore, 453 552, India

[b] Department of Mechanical Engineering, School of Technology, Pandit Deendayal Energy University, Raisan, Gandhinagar, 382 286, India

ARTICLE INFO

Keywords:
Plane moving wall
Tandem cylinders
Wake interference
Wall proximity
Vortex shedding suppression

ABSTRACT

Flow across tandem square cylinders placed close to a plane moving wall, has been studied extensively for various cylinder inter-spacing ratio ($0.5 \leq S/D \leq 8$) and cylinder-to-wall gap ratio values ($0.1 \leq G/D \leq 4$) at a fixed value of Reynolds number, $Re = 100$. Numerical experiments are performed using the computational package ANSYS FLUENT®. Results indicate that unsteady flow past tandem cylinders relies primarily on the presence of a moving wall. Exhaustive details on the effects of varying S/D and G/D values on the onset and suppression of vortex shedding behind the tandem cylinders are given. A detailed description of the underlying flow physics is provided through instantaneous vorticity and streamline contours. Forces such as the lift and drag acting on the cylinders are reasoned qualitatively through time-averaged pressure, lift, and drag coefficient plots. A remark on existence and suppression of flow unsteadiness is given through Strouhal number variation. A rigorous comparison of the present flow field with flow past an isolated square cylinder, square cylinder near a moving wall, and unbounded tandem cylinders is given. Overall, unlike the lift, drag coefficient values happen to be highest for single cylinder case, followed by the upstream cylinder, and they are least for the downstream cylinder.

1. Introduction

Buffeting of bluff bodies has always been a topic of interest for researchers as it has an immense pedagogic and practical importance. The flow field resulting from surrounding structures (another body or plane wall) is a complex scenario in the engineering field. Such instances can be modelled in their relevant bluff body analogies to understand the underlying flow physics with ease, *i.e.* tandem bluff bodies in proximity of a plane stationary/moving wall. The flow is governed by both the Reynolds number (Re) as well as the gap in individual bodies and wall. The onset and suppression of the vortex shedding observed from bluff bodies are of interest to researchers, as it as it influences the aerodynamics forces, vibration, heat as well as mass transfer [1]. Such occurrences are more prevailing in the fuel-saving intelligent transport system in automobiles [2], seabed pipelines with rough terrain ground [3–5], and tandem cyclists on racing track [6,7]. As mentioned earlier, one way to forecast the flow phenomenon in such cases is to understand the flow physics for simpler instances and attempt to find similar features with real-time applications.

Flow across tandem cylinders of various cross-sections as well as configuration have been studied extensively, especially the circular cylinder [8–14]. Flow patterns and the structure of wake around a cylinder with sharp corners, such as a square cylinder, vary

* Corresponding author.
E-mail addresses: sdhina@iiti.ac.in, ssdhinakar@gmail.com (S. Dhinakaran).

https://doi.org/10.1016/j.csite.2021.101042
Received 30 October 2020; Received in revised form 17 April 2021; Accepted 23 April 2021
Available online 29 April 2021

Nomenclature

$\overline{C}_{D1}$, $\overline{C}_{D2}$	time-averaged drag coefficient for upstream and downstream cylinder, respectively
$\overline{C}_{L1}$, $\overline{C}_{L2}$	time-averaged lift coefficient for upstream and downstream cylinder, respectively
C_D	drag coefficient, $F_D/(0.5\rho U_\infty^2 D)$
C_L	lift coefficient, $F_L/(0.5\rho U_\infty^2 D)$
C_P	pressure coefficient, $(p - p_\infty)/(0.5\rho U_\infty^2)$
f	frequency of vortex shedding, $1/t$
F_D	drag force, [N]
F_L	lift force, [N]
G	height of the gap between the cylinder and the wall, [m]
G/D	non-dimensional gap height from cylinder-to-wall
L	length of the boundary, [m]
m, n	number of grids in x- and y-directions, respectively
P	non-dimensional pressure, $p/(\rho U_\infty^2)$
p	dimensional pressure, [N m^{-2}]
Re	Reynolds number, $(\rho U_\infty D)/\mu$
S	inter-cylinder spacing distance between cylinders, [m]
S/D	non-dimensional inter-cylinder spacing distance between cylinders
St	Strouhal number, $(fD)/U_\infty$
T	Time period of vortex shedding
t	dimensional time, [s]
U	non-dimensional velocity in x-direction, u/U_∞
u, v	dimensional velocity in x- and y-directions, respectively, [m s^{-1}]
V	non-dimensional velocity in y-direction, v/U_∞
X	non-dimensional horizontal distance, x/D
x, y	horizontal and vertical coordinates, respectively
Y	non-dimensional vertical distance, y/D
AB, BC, CD, DA	front, bottom, rear and top faces of the upstream cylinder
D	height of the cylinder, [m]
EF, FG, GH, HE	front, bottom, rear and top faces of the downstream cylinder

Greek

Δ	largest grid size
δ	smallest grid size
μ	dynamic viscosity, [$kg\ m^{-1}$ s^{-1}]
ω	vorticity magnitude, [s^{-1}]
ρ	fluid density, [kgm^{-3}]
τ	non-dimensional time, $(tU_\infty)/D$

Subscript

0	reference value
∞	far field value
cl	central line
cr	critical value
ds	downstream
H	high value
h	height
l	local value of variable
M	mean value
us	upstream

considerably from that a circular cylinder due to fixed separation points, causing severe changes in critical flow regimes. Consider fluid flow across two identical square cylinders, which are arranged in tandem at a fixed inter-spacing ratio (S/D) and are placed in an unconfined domain. The flow remains fully attached to both the cylinders until $Re = 2$ as the single cylinder case [15]. Flow separation occurs at the rear corners of both the cylinders. Standing recirculation regions first form for the upstream cylinder between $1 \leq Re \leq 2$, while for the downstream cylinders they form between $2 \leq Re \leq 5$ [16]. Twin symmetric vortices are formed behind the cylinders beyond separation points and the recirculation length increases with Re as the vortices grow. It is seen that as the downstream cylinder gets closer to the upstream cylinder, the wake region of the upstream cylinder is comprised of two standing recirculation regions at the

front face of the downstream cylinder, which increases in size with decreasing S/D [17]. Stability of the vortices break, and they shed downstream alternatively beyond a particular critical value cylinder of inter-spacing ratio $(S/D)_{cr}$, for a given Reynolds number value. The amplitude and frequency of this shedding of vortices keep on rising with Reynolds number until $Re = 200$, beyond which the flow becomes three-dimensional. It is seen that this critical value is in inverse proportion with Re, but has better control on vortex shedding initiation/cessation. For example, at $S/D = 3$–4, vortex shedding occurs for $Re \geq 125$, while at $S/D = 4$–5, it occurs for $Re \geq 100$ [18, 19]. A positive jump, discontinuous in nature, has been reported for C_D of the downstream cylinder at critical gap ratio because of vortex impingement. It is seen that the vortex impingement behind the upstream cylinder generates significant fluid entrainment into the gap. As a result, the pressure gradient across both cylinders increases drastically [20]. Beyond this value of Re, the drag coefficient of the downstream cylinder approaches the corresponding value of the upstream cylinder. Also, the local minima are observed for frequency of vortex shedding, Strouhal number values close to $(S/D)_{cr}$. Generally, this happens due to the transition of gap flow from steady to unsteady flow regime, and the variation is seen much prominent for the downstream cylinder. Hence, S/D variation between the cylinder may promise interesting flow physics and the same is given in the literature. Most popularly, major flow regimes such as the single slender-body regime, reattachment regime, and co-shedding are identified [21–23]. As S/D value further increases, both the cylinders act as an isolated cylinder and there is no interference between their wake regions.

When the tandem arrangement of cylinders is brought in the vicinity of a stationary wall, the above-discussed flow physics alters drastically due to the interaction of a thick boundary layer on the wall with shear layer on cylinders. The stationary wall offers an irrational constraint to the cylinder wake, which eventually leads to suppression of vortex shedding below a critical cylinder-to-wall gap ratio (G/D) value. It should be mentioned that this entity again varies with Re and S/D values. As the tandem cylinders are brought near the wall, vortex shedding occurs, but in an upward biassed fashion. At broader inter-spacing ratio values (*i.e.*, $S/D \geq 3$), this pattern is more of impinging type, while for moderate to lower ratio values (*i.e.*, $1 \leq S/D \leq 3$), it is of reattachment type. At very low G/D values, periodic vortex shedding weakens and gets suppressed, as lower shear layer emanating from upstream cylinder keeps sticking to the stationary wall [24]. It is further seen that the upstream and downstream cylinders, in the presence of a stationary wall, shed vortices at the same frequency, but drag coefficient for the upstream cylinder is way higher than that of the downstream cylinder. Also, vortex shedding is delayed for the downstream cylinder, while it is needless to say that the critical Reynolds numerical values for the initiation of vortex shedding depends more on G/D [25].

As stated above, the stationary wall generates a local boundary layer around the cylinder, which complicates the flow physics even further, as the flow structure now depends on Re, G/D, and boundary layer properties. Hence, to simplify the problem, it can be assumed that the boundary layer moves at the same velocity as the far-field value. Such an understanding could facilitate the researcher to neglect the formation of the upstream boundary layer, to focus better on the influence of Re and G/D only, *i.e.* to study the near-wall effects. It has been noticed that limited information is available on the laminar flow past a two-dimensional circular (especially square) cylinder placed near a plane moving wall. D'Souza et al. [26] performed numerical simulations for flow across tandem circular cylinders near a moving wall at $Re = 200$. An early transition from intermediate to co-shedding phases was reported for $G/D = 0.5$ and $S/D = 2$ and 2.5. They suggest that a moving wall speeds up the onset of co-shedding for tandem cylinder

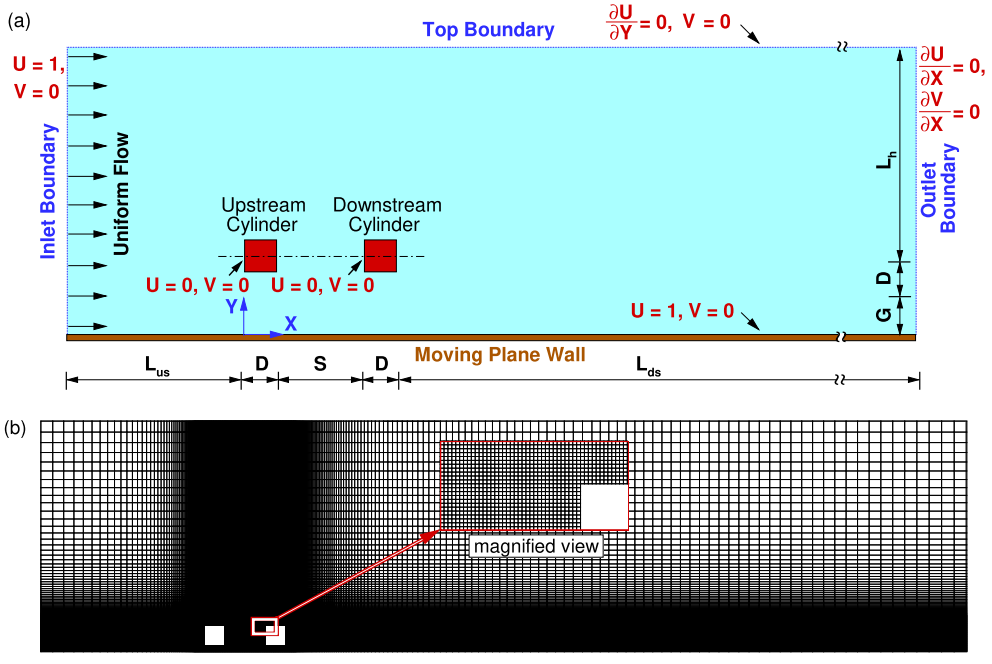

Fig. 1. (*a*) Schematic of the computational domain used in the present study; (*b*) sample grid distribution around the tandem cylinders at $G/D = 0.3$ with $S/D = 2.0$ configuration.

configuration. Perhaps the shielding effect of the upstream cylinder over downstream cylinder parameters exists for moving wall configuration, similar to the unconfined case. They suggest that cylinders behave like an isolated cylinder for $G/D \geq 0.5$. Bhattacharyya and Maiti [27] compared flow across a square cylinder placed in an unconfined domain with the proximity of a moving wall at $Re = 50$–1000 and $G/D = 0.5$, 0.25, and 0.1. It was found that a weak shear layer of negative vorticity, which forms due to the moving wall, affects vortex shedding downstream. Even at low values of gap ratio, vortex shedding suppression did not occur, unlike the stationary wall case. Far downstream, flow separation on the moving wall was reported. Dhinakaran [28] studied flow and heat transfer from a square cylinder in the vicinity of a plane moving wall. The simulations were performed for $Re = 100$ and $G/D = 0.1$–4. The author reported that the flow stays unsteady periodic for $0.4 \leq G/D \leq 4$, wherein two rows of vortex shedding exist for $1 \leq G/D \leq 4$, while a single row prevails for $0.4 < G/D < 1$. The vortex shedding gets completely suppressed below $G/D = 0.3$. Lift and drag coefficients increase with decreasing values of G/D.

From the above literature survey, it can be followed that not many numerical works are available on the flow around square cylinder near a moving wall. Moreover, tandem square cylinders near a moving wall is a topic that has not been explored yet. Primary goal of the present numerical endeavour is to study wall proximity and inter-cylinder spacing effects for different values of G/D ($\approx$ 0.1–4) and S/D ($\approx$ 0.5–0.8) ratios of tandem cylinder at $Re = 100$. Although the present study is two-dimensional and in the laminar flow regime, the computational results exhibits the flow field complexity with better efficacy.

2. Mathematical formulation

2.1. Problem description and geometrical configuration

As shown in Fig. 1 (a), two infinitely long stationary identical square cylinders of height D, are placed one behind the other (i.e., tandem arrangement) near a plane wall moving at the same velocity as the far-field velocity U_∞. The vertical distance between the bottom surface of the cylinder and the moving wall is defined as G, and the inter-cylinder spacing distance between two cylinders is defined as S. These distances are scaled with the characteristic length and are called cylinder-to-wall gap ratio, G/D, and inter-cylinder spacing ratio, S/D. G/D is varied between 0.1 and 0.6 in steps of 0.1 and further taken as 0.8, 1, 2 and 4. On the other hand, S/D is kept at 0.5, 6 and 8, and varied between 1 and 4 in the steps of 1.

The present study is fundamental and finds application in broad realms of engineering, including, but not limited to, wind and ocean engineering. During the parametric simulations, the Reynolds number is fixed at $Re = 100$, which is a typical value as far as theoretical analysis is considered. The primary focus is to discern flow physics, and the understanding provided applies to the 2D laminar unsteady flow regime. Hence, a representative value has been chosen where the Karman vortex sheet is distinctly visible. Since buffeted cylinders have been considered, the influence of spacing between the cylinders and the wall on the overall flow behaviour is the primary focus. Accordingly, the theoretical limits to mimic no gap and minimum gap have been considered, and the parameter ranges are chosen.

2.2. Governing equations

Equations governing the flow across tandem square cylinders viz., continuity and momentum (in the non-dimensional form) are given as.

Continuity equation:

$$\frac{\partial U}{\partial X} + \frac{\partial V}{\partial Y} = 0. \tag{1}$$

Momentum equations:

$$\frac{\partial U}{\partial \tau} + U\frac{\partial U}{\partial X} + V\frac{\partial U}{\partial Y} = -\frac{\partial P}{\partial X} + \frac{1}{Re}\left(\frac{\partial^2 U}{\partial X^2} + \frac{\partial^2 U}{\partial Y^2}\right), \text{and} \tag{2}$$

$$\frac{\partial V}{\partial \tau} + U\frac{\partial V}{\partial X} + V\frac{\partial V}{\partial Y} = -\frac{\partial P}{\partial Y} + \frac{1}{Re}\left(\frac{\partial^2 V}{\partial X^2} + \frac{\partial^2 V}{\partial Y^2}\right). \tag{3}$$

The above governing equations have been non-dimensionalised using: $X = \frac{x}{D}, Y = \frac{y}{D}, \tau = \frac{tU_\infty}{D}, P = \frac{p}{\rho U_\infty^2}, U = \frac{u}{U_\infty}, V = \frac{v}{U_\infty}$.

2.3. Boundary conditions

At the inlet boundary, a uniform flow profile (*i.e.*, $U_\infty = 1$, and $V = 0$) is assumed. A zero shear boundary condition is specified along the top boundary. *i.e.*, $\frac{\partial U}{\partial Y} = 0$, and $V = 0$. On the moving plane wall, a no-slip condition is applied and the wall moves at the same velocity as the far field (*i.e.*, $U_{(Y=0)} = 1$, and $V_{(Y=0)} = 0$). The right side boundary is designated as the outlet. The boundary located sufficiently far downstream from tandem cylinders and it is considered as the pressure outlet (*i.e.*, default option in FLUENT, known as 'PRESSURE OUTLET') which assumes a zero gauge (static) pressure (P) = 0 with respect to the operating pressure, $\frac{\partial U}{\partial X} = 0$, and $\frac{\partial V}{\partial X} = 0$ [29]. The no-slip wall condition (*i.e.*, U = 0, and V = 0) is applied on the cylinders' surface.

3. Numerical details

Numerical simulations are performed by utilising the commercial CFD package ANSYS FLUENT® [30]. FLUENT is based on the control volume technique for solving the governing partial differential equations. A pressure-based solver is used in which the pressure field is extracted by solving a pressure correction equation obtained by manipulating continuity and momentum equations. A two-dimensional, transient, laminar, viscous model, with double precision, is selected for modelling the flow at $Re = 100$. An implicit method is applied to obtain the discretised system of equations. The QUICK (Quadratic Upstream Interpolation for Convective Kinematics) scheme is selected for spatial discretisation of the convective terms and diffusion terms from equations [31]. The Semi-Implicit Method for Pressure Linked Equations (SIMPLE) algorithm is used for solving the governing equations with boundary conditions [32]. The PRESTO (PREssure STaggering Option) interpolation technique is utilised to obtain the values of face pressure from the values at the cell centre, and the second-order implicit scheme is used for transient formulation [33]. Iterations at each time step continue until a divergence-free velocity field is obtained. The optimum dimensionless time step size is taken as 0.0146. The convergence is assumed to be achieved when the summation of residuals are reduced to 10^{-6} for all the governing equations.

3.1. Grid dependence study

A rectangular computational domain is employed, as shown in Fig. 1 (a). In order to minimise the influence of boundary effects, the top lateral, inlet and outlet boundaries are placed sufficiently away from tandem cylinders. The inlet boundary lies at a distance (L_{us}) 8D from the front face of the upstream cylinder, while the top boundary is placed at a distance (L_h) 10D from the top face of the cylinders. These boundaries are kept sufficiently far away so that their presence does not hamper the flow physics. The influence of L_{ds} on $\overline{C}_{D1}$ and $\overline{C}_{D2}$ and Strouhal number (St) of the cylinder are tested for three distinct values of downstream length viz., 45D, 50D, and 55D.

As shown in Fig. 1 (b), a structured and non-uniform grid is used. The grid elements are sufficiently fine *i.e.*, $\delta = 0.01D$ and it is preferred among various element sizes: 0.015D, 0.01D, and 0.005D during grid-dependence study. This is evenly distributed over a distance of 0.5 units surrounding both the cylinders' surfaces and on the plane wall to attain a better description of wall-wake interactions. A non-uniform structured grid, with $\Delta = 0.25D$, is applied elsewhere. The grids are stretched by smooth transition using different bias factors *i.e.*, (growth rate) $^{(\text{number of divisions-1})}$.

For testing and assessing the grid-dependent solution, numerical experiments are carried out for several grid sizes for each value of G/D used in this study. For brevity, the test is presented, where the vortex shedding phenomenon exists and discussed here only at $G/D = 0.5$ with $S/D = 0.5$ and 8.0. Table 1 presents the effect of various grid size and downstream length (L_{ds}). Finally, downstream length 50D and grid 'E' is found to be an optimum choice providing best flow features, while incurring the comparatively less computational time and hence, it is being used for all the configurations of tandem cylinders.

3.2. Code verification

Firstly, code is verified with general case (*i.e.*, flow past an isolated square cylinder) of both the experimental and numerical data available in the literature, as shown in Table 2. For the main procedure of verifying the code, two different cases are solicited, namely unconfined cylinders, and cylinder close to a moving wall. As depicted in Fig. 2, the quantities such as $\overline{C}_D$ and St are compared to square cylinder near a moving wall case at $0.5 \leq G/D \leq 4.0$, and unbounded tandem cylinders case at $0.5 \leq S/D \leq 10$, at $Re = 100$ and they are compared with literature. Results of the present code are shown by a solid lines and the literature datas are shown by symbols. Similarly, closer to the present study as flow over a square cylinder near a moving wall are compared with Bhattacharyya and Maiti [27], Sharma and Eswaran [15], and Dhinakaran [28] at various G/D ratios. It is seen that a good agreement is obtained with the

Table 1
Grid sensitivity and downstream length (L_{ds}) dependence test on time averaged drag coefficient of tandem cylinders (*i.e.*, $\overline{C}_{D1}$ and $\overline{C}_{D2}$) and Strouhal number (St) at Reynolds number (Re) = 100 and cylinder-to-wall gap ratio (G/D) = 0.5.

L_{ds}	Grid (m × n)	$S/D = 0.5$			$S/D = 8.0$		
		$\overline{C}_{D1}$	$\overline{C}_{D2}$	St	$\overline{C}_{D1}$	$\overline{C}_{D2}$	St
	A (800 × 300)	1.8341	0.2196	0.1112	1.9852	0.7123	0.1392
45	B (1250 × 500)	1.8328	0.2187	0.1110	1.9851	0.7118	0.1390
	C (1650 × 700)	1.8290	0.2182	0.1109	1.9847	0.7120	0.1385
	D (800 × 320)	1.8273	0.2181	0.1106	1.9848	0.7119	0.1390
50[a]	E (1250 × 520)[a]	1.8271	0.2180	0.1105	1.9846	0.7117	0.1387
	F (1650 × 720)	1.8271	0.2180	0.1106	1.9846	0.7117	0.1386
	G (800 × 340)	1.8272	0.2183	0.1108	1.9850	0.7120	0.1387
55	H (1250 × 540)	1.8271	0.2180	0.1106	1.9848	0.7117	0.1387
	I (1650 × 740)	1.8271	0.2179	0.1105	1.9846	0.7116	0.1386

[a] Mesh and downstream length (L_{ds}) used in this study.

Table 2
Comparison of St and $\overline{C}_D$ with the literature at $Re = 100$.

Source	Study	St	$\overline{C}_D$
Okajima [37]	Experimental	0.141	–
Norberg [38]	Experimental	0.143	–
Davis et al [39].	2D, Numerical	0.165	1.63
Franke et al [40].	2D, Numerical	0.1538	1.61
Sahu et al [41].	2D, Numerical	0.1486	1.488
Saha et al [42].	3D, Numerical	0.151	1.504
Present	2D, Numerical	0.1512	1.51

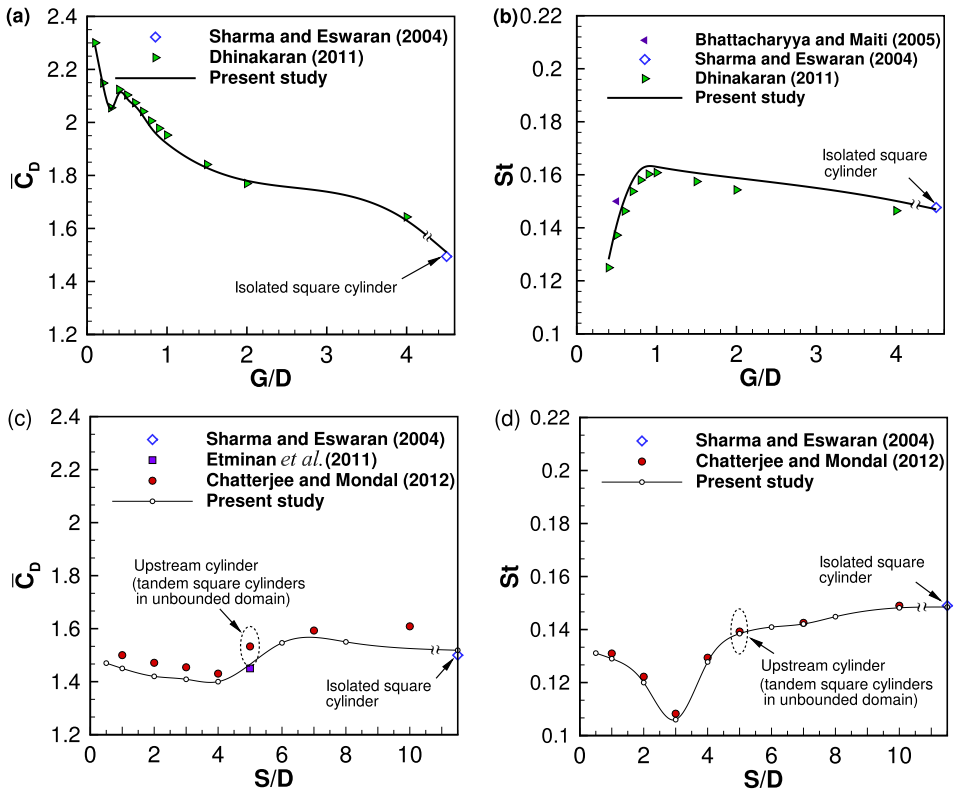

Fig. 2. Comparison of the computed average drag coefficient ($\overline{C}_D$), and Strouhal number (St) with those available in the literature at $Re = 100$. Subplots (a) and (b) depict flow past a square cylinder near a moving wall case. Subplots (c) and (d) depict flow around an unbounded tandem square cylinders case.

literature, and the same is shown in subplots (a) and (b). The results are found to be closer to those of Dhinakaran [28] with the maximum percentage of error 1.61% and 2.14% for $\overline{C}_D$ and St values, respectively. In another attempt to validate the code for the case of flow around unbounded tandem cylinders at various S/D values, $\overline{C}_D$ and St are plotted as depicted in subplots (c) and (d). The same is compared with available results of Sharma and Eswaran [15], Etminan et al. [34] and Chatterjee and Mondal [18]. Again, a good agreement is found with the literature, and the present results agree well with those of Chatterjee and Mondal [18] with the maximum percentage of error 3.87% and 2.11% under $\overline{C}_D$ and St values, respectively.

4. Results and discussions

In this study, the fluid flow across tandem cylinders of height, D, is investigated at various values of S/D and G/D at $Re = 100$. Effect of wall on the vortex shedding behind the tandem cylinders is analysed at various gap ratio values: $G/D = 0.1$, 0.2, 0.3, 0.4, 0.5, 0.6, 0.8, 1, 2, and 4, and $S/D = 0.5$, 1, 2, 3, 4, 6, and 8. Details of the numerical results are presented in the sections to follow.

4.1. Vortex shedding cycle: instantaneous vorticity contours

When fluid flows past tandem square cylinders lying close to a plane moving wall, flow physics gets quite complicated due to the interaction of cylinders' wake region and gap flow between cylinders and the moving wall. Vortex shedding occurs downstream side of the cylinders near the moving wall, as shown in Fig. 3, wherein vorticity contours are presented for a cycle of lift coefficient oscillation for $S/D = 8.0$ and 0.5, and $G/D = 4.0$ and 0.5. The subplot (a) represents the time history of lift coefficient for the upstream cylinder. Subplots (b) - (e) depict vortex shedding cycle at various time stamps A, B, C, and D marked on lift coefficient (C_L) oscillation curve in the subplot (a). When the cylinders are far away from each other ($S/D = 8.0$) and the moving wall ($G/D = 4.0$), shear layers originating from the upstream cylinder, which break after rolling up, impinge on the front face of the downstream cylinder. The detached or shed vorticity partially merges with the shear layer of the downstream cylinder of the same kind (positive with positive and negative with negative). Such an occurrence is seen to take place between time instants C and D in subplot (b). As a result, two changes occur in hydrodynamics of the downstream cylinder. Firstly, the vorticity pattern of the downstream cylinder spreads transversely, and immediate separation of vortices occurs, primarily due to the overwhelmed strength of the respective shear layer. Secondly, the shed vorticity encapsulates almost the entire cylinder, causing pressure distribution around the cylinder experience significant drift, and hence, the lift and drag forces vary significantly. While the lift force acting on the downstream cylinder should rise due to increased growth of shear layer, the drag force reduces because of the same reason. As the cylinders move towards each other (shown in Fig. 4), for the same G/D value, the shear layers of the upstream cylinder interfere more with those of the downstream cylinder, even before separating into blobs, which is seen in subplots (a), (d), and (g) for instance. However, the above phenomenon persists, with the transverse width of the shear layers at the downstream cylinder to be shrunken and the vortex street to be more regular (shown in subplots (c) and (e)). The gap vortices between the upstream and downstream cylinders continue to merge with a shear layer of the downstream cylinder and aid the growth of vortex shedding (unsteady flow persists), causing C_L oscillation to further increase in amplitude. As the cylinders further move towards each other ($S/D = 0.5$), gap flow regime becomes quasi-steady, and weak shedding of vortices is witnessed, wherein the shear layers stretch downstream without rolling up to a greater extent. Here, both the cylinders seem virtually like a single cylinder and the vortices are shed mostly from the downstream cylinder, as displayed in subplots (c) and (e).

For a lower value of G/D, the vortex shedding trend is different from higher G/D ratio values ($G/D \geq 2$), and the details can be seen in Fig. 4(b), (c), (e), (f), (h), and (i). At $S/D = 6.0$, the negative shear layer emanating from the upper side of the upstream cylinder plays a dominant role in the entire shedding process. Secondary vortices are induced at the moving wall due to these primary vortices.

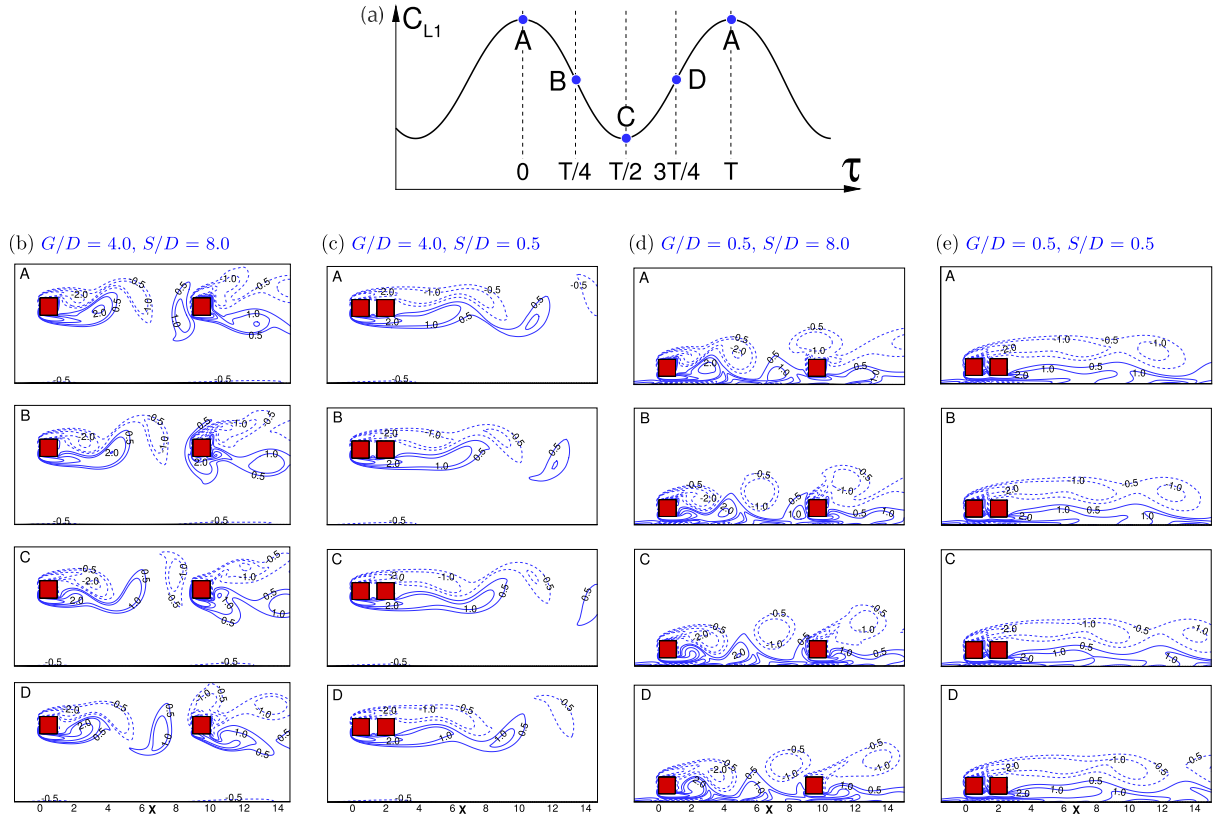

Fig. 3. Vorticity contours for (a) one cycle at different time instants (A, B, C, and D) are plotted for various G/D and S/D values. At $G/D = 4.0$ with (b) $S/D = 8.0$ and (c) $S/D = 0.5$. At $G/D = 0.5$ with (d) $S/D = 8.0$ and (e) $S/D = 0.5$.

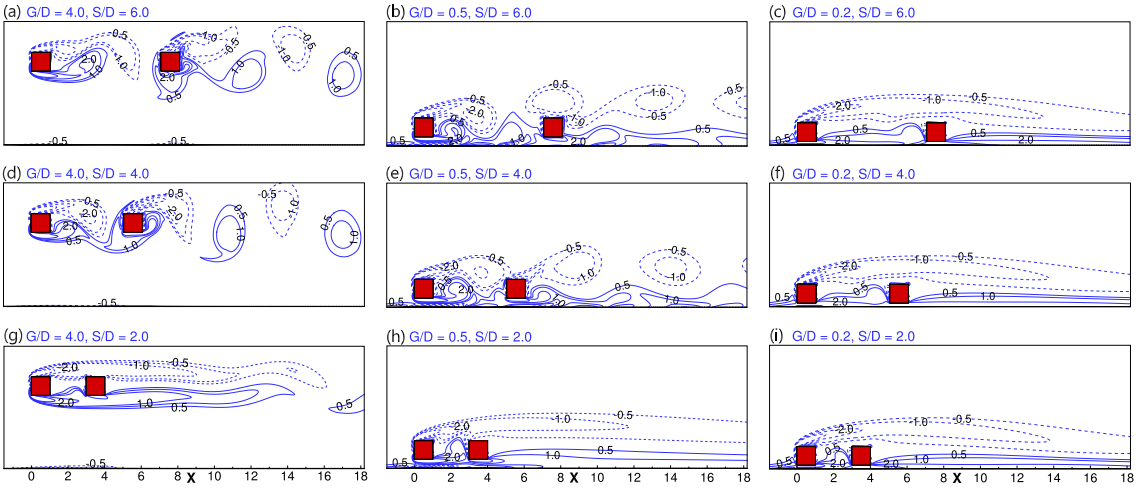

Fig. 4. Instantaneous vorticity contours in the wake of tandem cylinders at $G/D = 4.0$, 0.5, and 0.2, and $S/D = 6.0$, 4.0, and 2.0. The contours are presented at same non-dimensional time.

Later, this secondary vorticity gets convected downstream along with the flow between two primary vortices. Both, primary as well as secondary vorticity, impinge on the front surface of the downstream cylinder into an asymmetrical vortex pair and then move downstream as a single shed vortex. This phenomenon exists until the cylinders are brought closer to each other ($S/D = 2.0$), wherein quasi-steady flow appears between cylinders that were mentioned earlier. The primary vortex becomes stronger and does not roll-up downstream, but instead stretches itself in the direction of flow, along with the secondary vortex. The reason for such an occurrence is that two shear layers which separate from the upstream cylinder reattach on the downstream cylinder, which can be viewed in subplots (h) and (i). Significant reduction in vortex shedding intensity is apparent due to the weak separation of vortices at distant downstream. Again, vortices are shed dominantly from the upstream cylinder unlike at intermediate values of S/D.

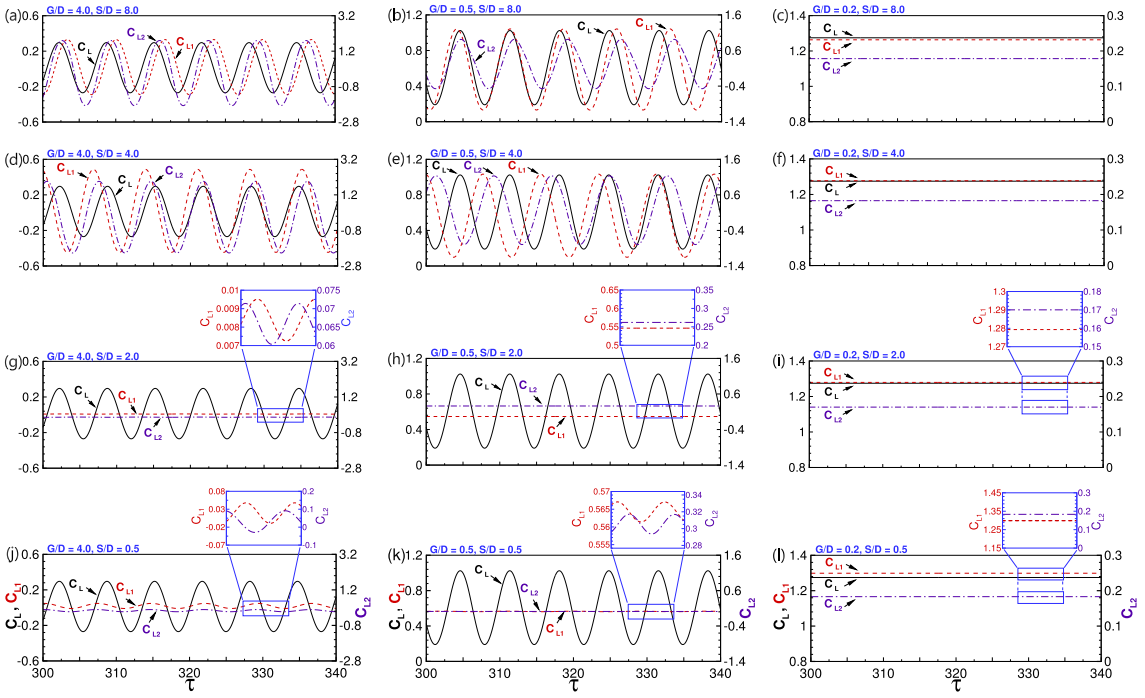

Fig. 5. Time evolution of lift coefficients of upstream (C_{L1}) and downstream (C_{L2}) cylinders represented by dotted and dash-dotted lines, respectively, at different values of G/D and S/D. The lift coefficient of single cylinder (C_L) for respective G/D values is shown through the solid line.

4.2. Time evolution of lift and drag coefficients

Time variation of lift and drag coefficients are shown in Figs. 5 and 6. When the tandem cylinders are well above the moving wall (*i.e.*, $G/D = 4.0$) and far away from each other (*i.e.*, $S/D = 8.0$), the upstream cylinder seems to be acting like a single isolated cylinder. The flow oscillations for the downstream cylinder appear higher than those for the single cylinder and upstream cylinder. At $G/D = 0.5$, when the cylinders are brought closer, *i.e.* S/D is reduced, the periodicity of the lift forces acting on the upstream cylinder tends to sync with the downstream cylinder (*i.e.*, $S/D = 4.0$) until it gets suppressed at $S/D \geq 2.0$. Such an occurrence suggests cancelling of shear layers between individual cylinders, and cylinder and moving wall. However, as S/D is further reduced, weak oscillations in C_L curve emerge for both cylinders, which has been highlighted separately in subplots (g), (j) and (k). When these tandem cylinders move closer to the moving wall, *i.e.* G/D is reduced, a jump is seen in the amplitude of oscillation. On the other hand, when these cylinders are brought very close to the moving wall, clear suppression of vortex shedding is apparent at $G/D = 0.2$.

In Fig. 6, the time evolution of drag coefficient is displayed at $G/D = 4.0$ and 0.5, and $S/D = 8.0$, 4.0, and 2.0. It is seen that at $G/D = 4.0$, the time evolution of drag coefficient curve has two peaks in the region of $S/D \geq 4.0$ and the oscillations occur at twice the vortex shedding frequency, and it completely vanishes at $S/D = 3.0$ and below. When the cylinders are brought closer to the wall, *i.e.*, G/D is reduced, the curve has a single peak, and it oscillates with the almost same frequency in the range $S/D \geq 4.0$. This periodicity of curve disappears at $S/D < 4.0$ for tandem cylinders. At $G/D = 0.2$, C_D and C_{D1} curves oscillate nearly with the same magnitude, and it is higher than C_{D2}. Results of above flow interactions on the vortex shedding behind the cylinder can be understood further through vortex shedding frequency plots given below.

4.3. Strouhal number

For providing further insight into existence or suppression of vortex shedding, the Strouhal number variation at various S/D and G/D values are given in Fig. 7. Strouhal number, given as St ($= fD/U_\infty$), is a measures the vortex shedding frequency of oscillating flow [35]. The vortex shedding frequency, f, is calculated by taking the reciprocal of the time interval between two subsequent vortex shedding cycles (measured from the lift coefficient oscillations). It should be noted that St values have been given for the upstream cylinder in particular. Also, St value is the same for both cylinders and moving wall. As seen earlier, when the cylinders are moved closer for a given G/D value, impinging vortices turn into reattaching vortices and further, the unsteady gap flow dynamics turns quasi-steady. As a result, a decline occurs in St values up to $S/D = 3.0$, followed by the jump in St values which continues until $S/D = 0.5$. Perhaps, such a jump can be ascertained to the rising tendency of tandem cylinders to act as a single cylinder, due to the declined

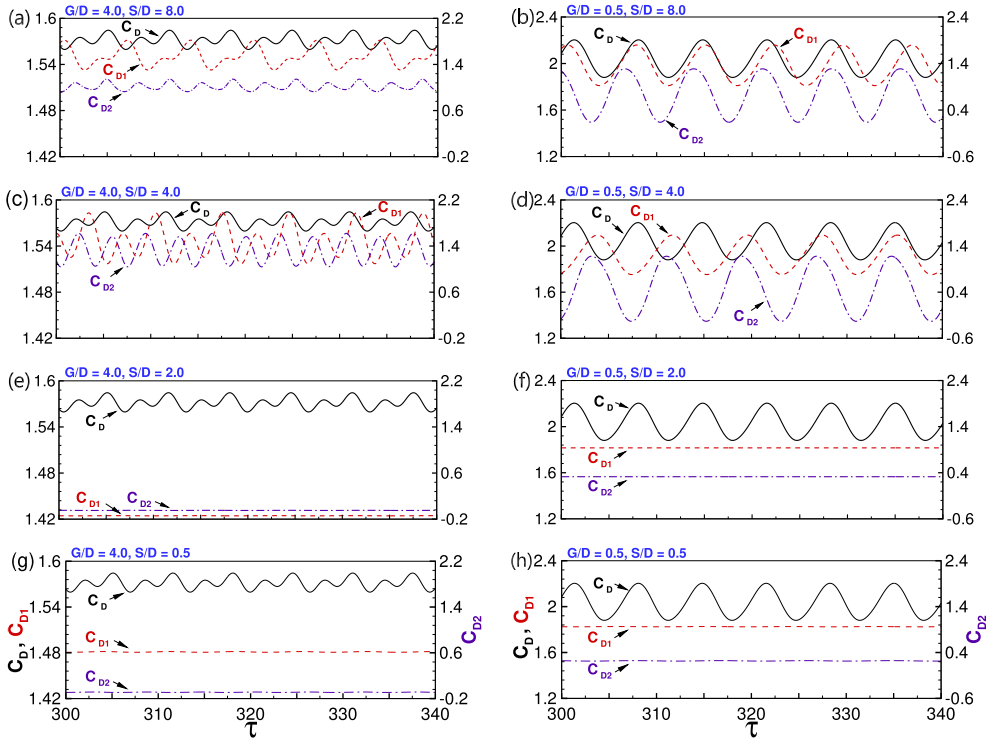

Fig. 6. Time evolution of drag coefficients of upstream (C_{D1}) and downstream (C_{D2}) cylinders represented by dotted and dash-dotted lines, respectively, at different values of G/D and S/D. The drag coefficient of single cylinder (C_D) for respective G/D values is shown through the solid line.

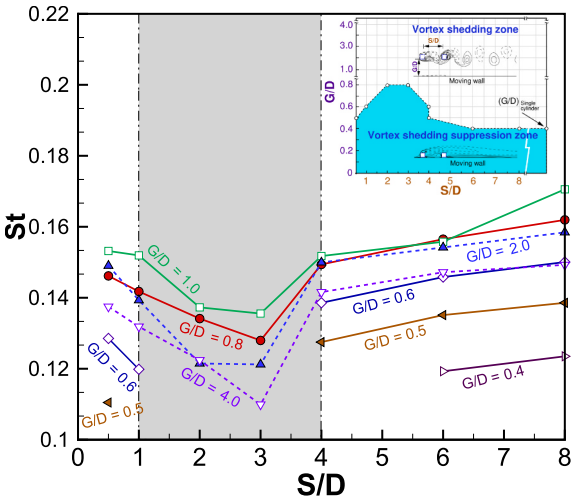

Fig. 7. Dependence of Strouhal number (St) on the cylinder-to-wall gap ratio (G/D) and inter-cylinder spacing ratio (S/D) of tandem cylinders. The subplot depicts typical zones of vortex-shedding based on G/D and S/D values. The highlighted portion stresses on the major changes in the flow field pertaining to unsteadiness of the fluid flow.

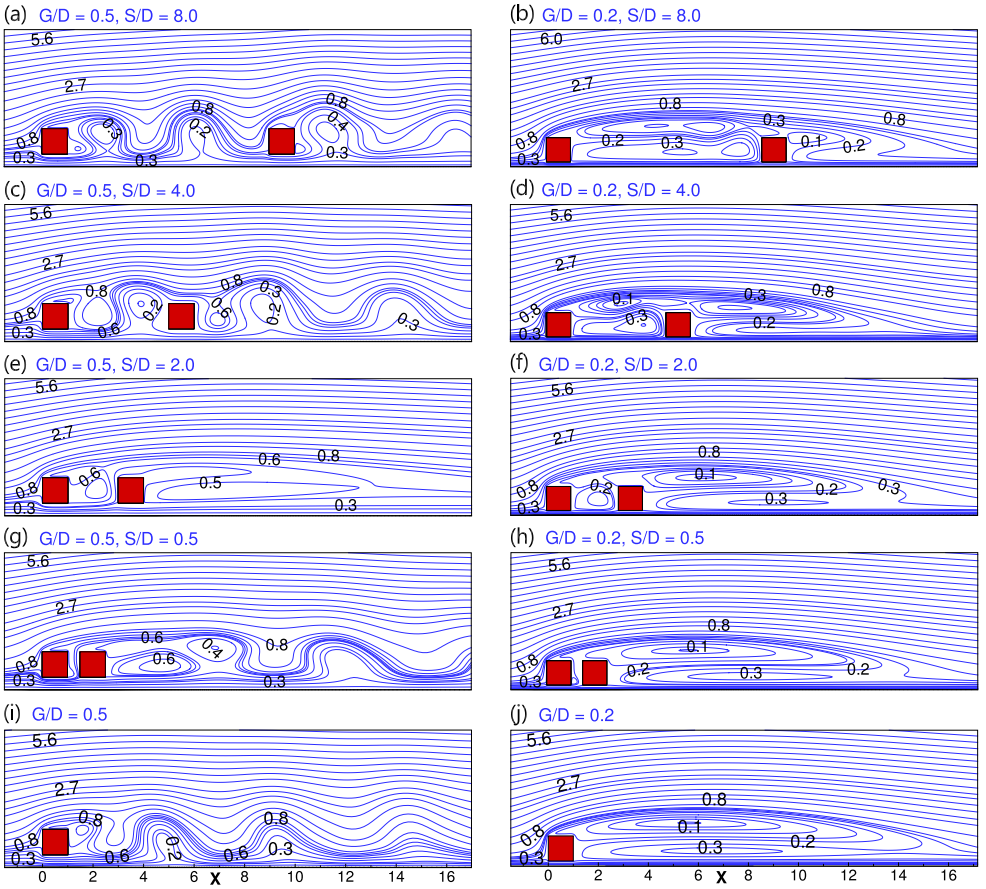

Fig. 8. Instantaneous streamline contours in the wake of tandem cylinders at $G/D = 0.5$ and 0.2 for different values of S/D. The contours are presented at same non-dimensional time.

gap flow dynamics. More flow separation and vortex shedding begin to occur beyond the downstream cylinder, and both the cylinders start acting like a single cylinder as discussed above.

Again, the jump in St exists when the cylinders are brought near the moving wall for a given value of S/D as well. In this case, initially St increases upto $G/D = 1.0$, and further, it decreases until the complete suppression of vortex shedding. This transition happens when the secondary vortex on the moving wall builds entirely from the bottom shear layer due to the primary vortex emerging from the upper end of the upstream cylinder. At very close proximity to the moving wall, as shown before, negative shear layer from the top end of cylinders convects downstream without or with less rolling and stretches along with the flow. Resultingly, a decline in the Strouhal number values is seen.

There exist critical G/D and S/D values beyond which the vortex shedding suppresses. As shown in the subplot, for $G/D = 4.0$–0.8, the flow remains unsteady for all values of S/D. However, for $G/D = 0.6$, vortex shedding gets suppressed between $1 < S/D < 4$, while for $G/D = 0.5$, this range gets stretched to $0.5 < S/D < 4$. At $G/D = 0.4$, vortex shedding ceases to exist for $S/D > 6$. At even lesser G/D values of 0.3, 0.2, and 0.1, flow across tandem cylinders remains steady for all values of S/D.

4.4. Instantaneous streamlines contours

In continuation to the above discussion, focussing on flow across tandem cylinders closer to the moving wall, instantaneous streamline contours are plotted in Fig. 8. At $G/D = 0.5$, the existence of von Karman vortex street and shedding of vortices behind the cylinders at these gap heights is lucid from the subplots (a), (c), (e), (g), and (i). When cylinders are far from each other (*i.e.*, $S/D = 8.0$ and 4.0), an asymmetric but identifiable vortex shedding persists (shown in subplots (a) and (b)). Later, at $S/D = 2.0$, displayed in subplots (e) and (f), vortex shedding is seen to be suppressed along with a standing asymmetric wake which encapsulates both the cylinders. The flow field is characterised by two recirculation regions behind both the cylinders. The one behind the upstream cylinder is more skewed and is weak due to the shorter gap flow region, while the one behind the downstream cylinder is less skewed and longer. Both these recirculation regions together form a large recirculation in the wake region that emerges from the top corner of the front face of the upstream cylinder. Such a wake has also been seen before for a single cylinder near the moving wall [28]. However, as the distance between the cylinders is further reduced to $S/D = 0.5$, the stability of this long recirculation breaks and unsteadiness is evident through weak oscillations in the flow behind the cylinders, as already discussed before. Such an occurrence can indicate the tendency of tandem cylinders to act as a single cylinder at this S/D value. A comparison is shown between subplots (g) and (i), and (h) and (j).

When the cylinders are brought very near to the wall (*i.e.*, $G/D = 0.2$), the flow remains steady for all values of S/D. The flow field is characterised by the same long-standing wake region, with two asymmetric recirculation behind each cylinder. The length of these

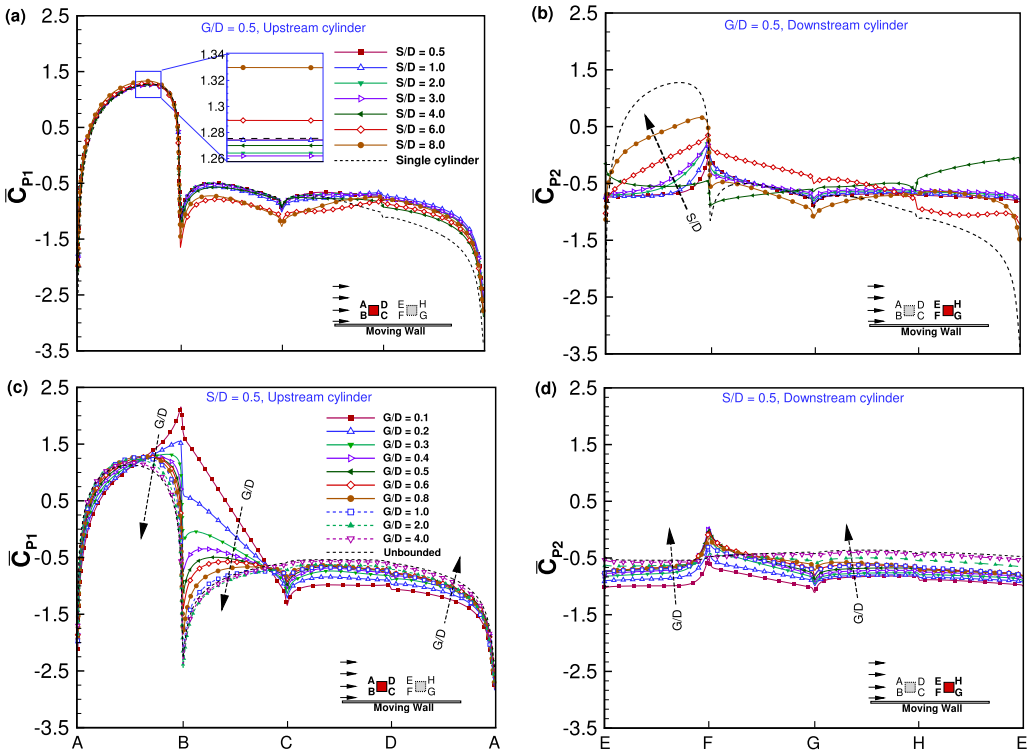

Fig. 9. Time-averaged pressure distribution coefficient along the surface of upstream ($\overline{C}_{P1}$) and downstream ($\overline{C}_{P2}$) cylinders. (*a*) and (*b*); at a fixed cylinder-to-wall gap ratio. (*c*) and (*d*); at a fixed inter-cylinder spacing ratio.

recirculation regions depends on both S/D and G/D values. It is apparent that as the gap between the cylinders decreases, the wake behind the downstream cylinder increases in length, while it decreases between the cylinder. Also, when the cylinders move closer to the moving wall, the recirculation region increases in length, as shown for $S/D = 0.5$ (shown in subplot (h)). Implications of the same on pressure field across the cylinders, which in turn affects the lift and drag forces are given in the section to follow.

4.5. Time-averaged pressure coefficient

Gap flow between the cylinders, and the cylinders and the moving wall, can be further understood through the distribution of coefficient of pressure over individual cylinders shown in Fig. 9. It should be noted that the pressure difference across the opposite faces of the cylinder results in the net lift and drag forces acting across the bodies. At $G/D = 0.5$, influence of S/D on $\overline{C}_{P1}$ is shown in subplot (a). It is clear that for the upstream cylinder, $\overline{C}_{P1}$ varies a little for various S/D values. The pressure distribution is qualitatively similar to a single-cylinder case, wherein the pressure is maximum and positive on the frontal face due to smooth incoming flow and existence of the stagnation point. On the other hand, $\overline{C}_{P2}$ shows significant variations on EF, EH and FG faces, which can be seen in subplot (b). The occurrence is in coherence with the understanding that as the gap between upstream and downstream cylinders is reduced, especially in the single-cylinder like (high S/D) and re-attachment regimes (intermediate S/D), the downstream cylinder receives disturbed flow. The phenomenon has already been visualised through vorticity and streamline contours in the previous sections. Furthermore, due to impinging vortices on *EH* and *FG* faces, a jump is seen in $\overline{C}_{P2}$ value until the vortices reattach at $S/D = 4.0$, below which $\overline{C}_{P1}$ decreases and remains almost unchanged. Maximum pressure values are found on the frontal faces of both the cylinders. Moreover, the minimum pressure value occurs at the A and E corner of upstream and downstream cylinders, respectively, which are the initiation points for vortex shedding.

Similarly, for a given spacing ratio, $S/D = 0.5$, the influence of G/D is shown in subplots (c) and (d), for upstream and downstream cylinders, respectively. Much different are the effects of decreasing gap ratio values on pressure distribution along with the individual cylinders, for the same S/D value. A sharp jump in the $\overline{C}_{P1}$ value is seen at the corner B, and a mild variation at the corner F, because of the confluence of primary and secondary vortices at this location, respectively, wherein moving wall presence is seen. Therefore, at faces AB and BC, $\overline{C}_{P1}$ increases drastically as the tandem cylinders shift near the moving wall. Unlike S/D variation, the gap between the cylinder and moving wall appear to affect flow features most for the upstream cylinder. As shown in subplot (d), $\overline{C}_{P2}$ reduces with G/D, mostly because of suppressed vortex shedding and the asymmetric wake engulfing the downstream cylinder. In short, when G/D is reduced, the pressure coefficient of downstream cylinder remains lesser than that of the upstream cylinder.

4.6. Time-averaged lift and drag coefficients

Variation of time-averaged C_L and C_D is shown in Fig. 10, respectively. As shown in subplot (a,d) of both Fig. 10, the pressure coefficient distribution detailed above indicates clearly that lift and drag forces for upstream cylinder must be closer to the single cylinder and that the downstream cylinder must have lesser values for the same. As indicated in subplots (b,e) and (c,f), with varying S/D, not much variation occurs in both lift and drag coefficients for the upstream cylinder, whereas for the downstream cylinder this may be more variant. These presumptions based on $\overline{C}_P$ distribution hold true. Also, for the upstream cylinder, a monotonous rise in both $\overline{C}_{L1}$ and $\overline{C}_{D1}$ with reducing G/D for various S/D values is not surprising. The pressure gradient across the front and rear, and top and bottom faces increases as the upstream cylinder is moved closer to the wall. For the downstream cylinder, $\overline{C}_{L2}$ and $\overline{C}_{D2}$ show quite an erratic pattern, which is not uncommon [18,22,26,36]. Such an occurrence can be credited to the incoming disturbed flow past the upstream cylinder, different types of vortex shedding patterns (impinging, reattaching and quasi-steady vortices), and the presence of a moving wall in the close proximity of the tandem cylinders. It is seen that lift and drag coefficient values are higher for the upstream cylinder, followed by single cylinder case and least for the downstream cylinder at $G/D = 0.5$. Hence, when a square cylinder is buffeted behind another square cylinder, and if they are travelling with the same speed, a lesser drag force and stable flow across it can be assured for specific gap ratio values. The principle is often put to use in intelligent fuel transport system as mentioned during the applications of buffeting [2].

5. Conclusions

Flow across tandem cylinders near a wall is explored numerically for various cylinder-to-wall gap ratio ($0.1 \leq G/D \leq 4.0$) and inter-cylinder spacing ratio values ($0.5 \leq S/D \leq 8.0$) at Reynolds number (Re) = 100. The moving wall plays a predominant role in altering the flow dynamics around and between the tandem cylinders at different gap spacing ratios. Computational results suggest that the gap between the moving wall and the tandem cylinders is more dominant in the suppression of vortex shedding than the space between the cylinders. Details on the critical values of G/D and S/D for suppression of unsteady flow are provided. For $G/D = 4.0$–0.8, the flow remains unsteady for all values of S/D. For $G/D = 0.6$, vortex shedding gets suppressed between $1.0 < S/D < 4.0$. For $G/D = 0.5$, this range gets extended to $0.5 < S/D < 4.0$. At $G/D = 0.4$, vortex shedding no longer exists for $S/D < 6.0$. At $G/D = 0.3$, 0.2, and 0.1, flow across tandem cylinders remains steady for all values of S/D. Furthermore, rigorous details on the existence and suppression of flow unsteadiness is given through Strouhal number variation. C_D and C_L show a regular pattern for the upstream cylinder, while a chaotic trend for downstream cylinder appears due to the incoming disturbed flow past the upstream cylinder, various types of vortex shedding patterns (impinging, reattaching and quasi-steady vortices), and the presence of moving wall. Overall, unlike the lift, drag

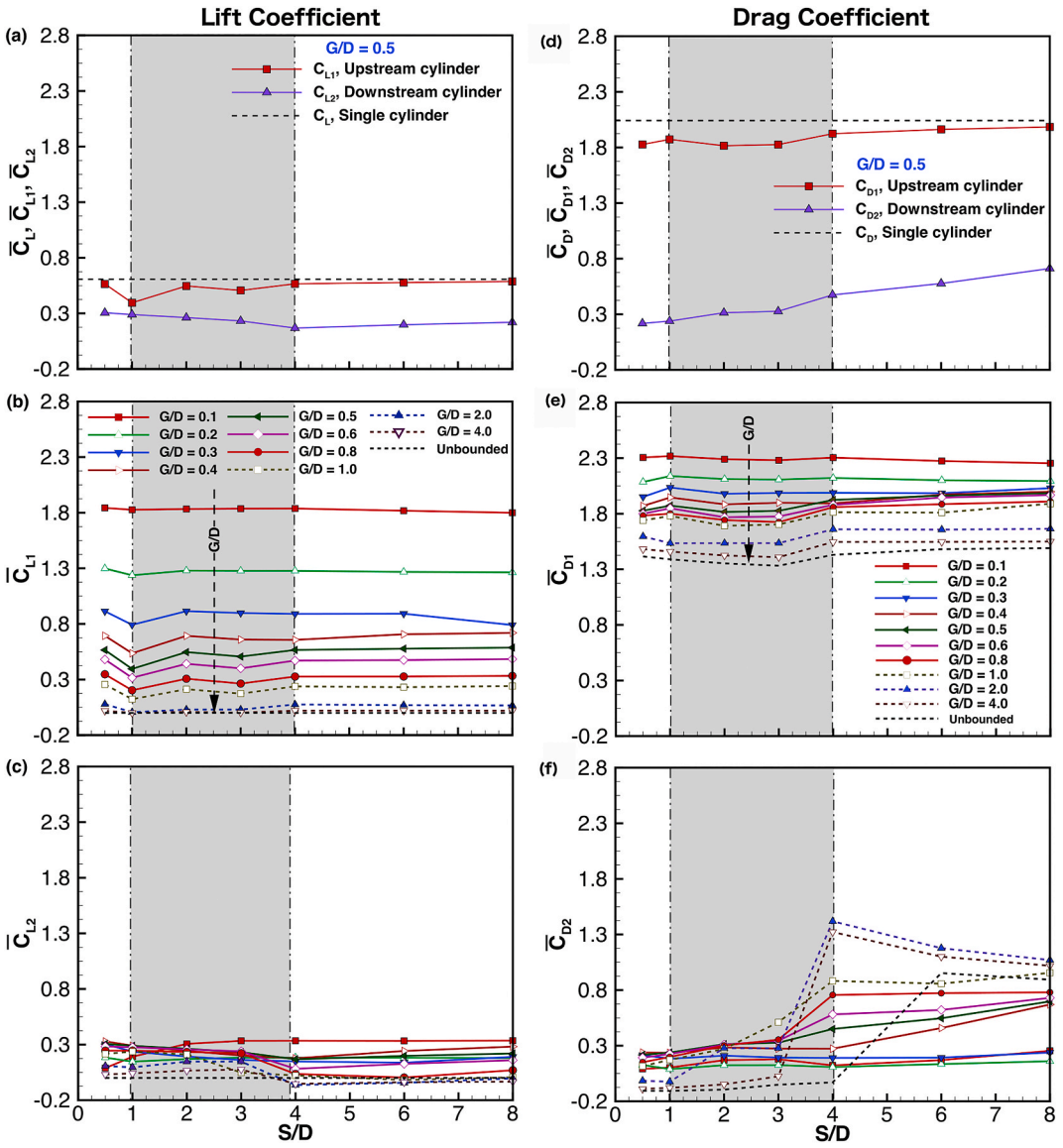

Fig. 10. Comparison of time-averaged (a) lift and (d) drag coefficient of upstream ($\overline{C}_{L1}$ & $\overline{C}_{D1}$) and downstream ($\overline{C}_{L2}$ & $\overline{C}_{D2}$) cylinders as a function of inter-cylinder the spacing ratio (S/D) at fixed cylinder-to-wall gap ratio (G/D) = 0.5 with reference to individual lift and drag coefficient of a single ($\overline{CL}$ & $\overline{CD}$) cylinder at same G/D. Time-averaged (b) lift ($\overline{C}_{L1}$) & (e) drag ($\overline{C}_{D1}$) coefficient of upstream cylinder and time-averaged (c) lift ($\overline{C}_{L2}$) & (f) drag ($\overline{C}_{D2}$) coefficient of downstream cylinder as a function of S/D, and compared with unbounded tandem cylinders case at the same S/D value.

coefficient values are highest for a single cylinder, followed by the upstream cylinder, and they are least for the downstream cylinder. Hence, for a certain range of spacing ratios mentioned earlier, the buffeting of the square cylinder is recommended for applications in wind and ocean engineering field.

References

[1] T. Nishino, G.T. Roberts, X. Zhang, Vortex shedding from a circular cylinder near a moving ground, Phys. Fluids 19 (2) (2007), 025103.
[2] F. Browand, J. McArthur, C. Radovich, Fuel Saving Achieved in the Field Test of Two Tandem Trucks, Partners for Advanced Transit and Highways (PATH) Program, 2004, pp. 1–28. Technical Report for Tesk Order-4214, California, ISSN 1055-1425.
[3] M. Zdravkovich, Forces on a circular cylinder near a plane wall, Appl. Ocean Res. 7 (4) (1985) 197–201.
[4] B. Yang, F.-P. Gao, Y.-X. Wu, D.-H. Li, Experimental study on vortex-induced vibrations of submarine pipeline near seabed boundary in ocean currents, China Ocean Eng. 20 (1) (2006) 113.
[5] F.-P. Gao, B. Yang, Y.-X. Wu, S.-M. Yan, Steady current induced seabed scour around a vibrating pipeline, Appl. Ocean Res. 28 (5) (2006) 291–298.
[6] N. Barry, J. Sheridan, D. Burton, N.A. Brown, The effect of spatial position on the aerodynamic interactions between cyclists, Procedia Engineering 72 (2014) 774–779.

[7] N. Barry, D. Burton, J. Sheridan, M. Thompson, N.A. Brown, Flow field interactions between two tandem cyclists, Exp. Fluid 57 (12) (2016) 181.
[8] L. Wang, M. Alam, Y. Zhou, Two tandem cylinders of different diameters in cross-flow: effect of an upstream cylinder on wake dynamics, J. Fluid Mech. 836 (2018) 5–42.
[9] W. Yang, M.A. Stremler, Critical spacing of stationary tandem circular cylinders at Re=100, J. Fluid Struct. 89 (2019) 49–60.
[10] X. He, S. Ali, H. Jing, Energy transmission at subcritical Reynolds numbers for the wake-induced vibration of cylinders in a tandem arrangement, Ocean. Eng. 211 (2020) 107572.
[11] N. Hosseini, M.D. Griffith, J.S. Leontini, The flow past large numbers of cylinders in tandem, J. Fluid Struct. 98 (2020) 103103.
[12] S. Sarkar, C. Mondal, N.K. Manna, S.K. Saha, Forced convection past a semi-circular cylinder at incidence with a downstream circular cylinder: thermofluidic transport and stability analysis, Phys. Fluids 33 (2020), 023603.
[13] W. Chen, C. Ji, D. Xu, Z. Zhang, Vortex-induced vibrations of two inline circular cylinders in proximity to a stationary wall, J. Fluid Struct. 94 (2020) 102958.
[14] M. Zhao, Flow past a circular cylinder and a downstream sphere for Re $<$ 300, J. Fluid Mech. 913 (2021) A20.
[15] A. Sharma, V. Eswaran, Heat and fluid flow across a square cylinder in the two-dimensional laminar flow regime, Numer. Heat Tran., Part A: Applications 45 (3) (2004) 247–269.
[16] A. Sohankar, A. Etminan, Forced-convection heat transfer from tandem square cylinders in cross flow at low Reynolds numbers, Int. J. Numer. Methods Fluid. 60 (7) (2009) 733–751.
[17] D. Chatterjee, G. Biswas, The effects of Reynolds and Prandtl numbers on flow and heat transfer across tandem square cylinders in the steady flow regime, Numer. Heat Tran., Part A: Applications 59 (6) (2011) 421–437.
[18] D. Chatterjee, B. Mondal, Forced convection heat transfer from tandem square cylinders for various spacing ratios, Numer. Heat Tran., Part A: Applications 61 (5) (2012) 381–400.
[19] W. Zhang, H.-S. Dou, Z. Zhu, Y. Li, Unsteady characteristics of low-Re flow past two tandem cylinders, Theor. Comput. Fluid Dynam. 32 (4) (2018) 475–493.
[20] Q. Shui, C. Duan, D. Wang, Z. Gu, New insights into numerical simulations of flow around two tandem square cylinders, AIP Adv. 11 (2021), 045315.
[21] W.S. Abbasi, R. Mahmoud, A. Naheed, On the wake interference effects for flow around tandem bodies, J. Braz. Soc. Mech. Sci. Eng. 42 (2020) 53.
[22] A. Sohankar, A numerical investigation of the flow over a pair of identical square cylinders in a tandem arrangement, Int. J. Numer. Methods Fluid. 70 (10) (2012) 1244–1257.
[23] A. Sohankar, E. Rangraz, M. Khodadadi, M. Alam, Fluid flow and heat transfer around single and tandem square cylinders subjected to shear flow, J. Braz. Soc. Mech. Sci. Eng. 42 (2020) 414.
[24] X. Wang, Z. Hao, J.-X. Zhang, S. Tan, Flow around two tandem square cylinders near a plane wall, Exp. Fluid 55 (10) (2014) 1818.
[25] A. Harichandan, A. Roy, Numerical investigation of flow past single and tandem cylindrical bodies in the vicinity of a plane wall, J. Fluid Struct. 33 (2012) 19–43.
[26] J.E. D'Souza, R.K. Jaiman, C.K. Mak, Dynamics of tandem cylinders in the vicinity of a plane moving wall, Comput. Fluids 124 (2016) 117–135.
[27] S. Bhattacharyya, D. Maiti, Vortex shedding from a square cylinder in presence of a moving wall, Int. J. Numer. Methods Fluid. 48 (9) (2005) 985–1000.
[28] S. Dhinakaran, Heat transport from a bluff body near a moving wall at Re = 100, Int. J. Heat Mass Tran. 54 (25) (2011) 5444–5458.
[29] C. Sasmal, R. Chhabra, Laminar natural convection from a heated square cylinder immersed in power-law liquids, J. Non-Newtonian Fluid Mech. 166 (14–15) (2011) 811–830.
[30] A.F. Ansys, 14.0 Theory Guide, ANSYS INC, 2011, pp. 218–221.
[31] B.P. Leonard, A stable and accurate convective modelling procedure based on quadratic upstream interpolation, Comput. Methods Appl. Mech. Eng. 19 (1) (1979) 59–98.
[32] S. Patankar, D. Spalding, A calculation procedure for heat, mass and momentum transfer in three-dimensional parabolic flows, Int. J. Heat Mass Tran. 15 (10) (1972) 1787–1806.
[33] S. Patankar, Numerical Heat Transfer and Fluid Flow, CRC press, 1980.
[34] A. Etminan, M. Moosavi, N. Ghaedsharafi, Determination of flow configurations and fluid forces acting on two tandem square cylinders in cross-flow and its wake patterns, Int. J. Mech. 5 (2011) 63–74.
[35] P.W. Bearman, Vortex shedding from oscillating bluff bodies, Annu. Rev. Fluid Mech. 16 (1) (1984) 195–222.
[36] S. Bhattacharyya, S. Dhinakaran, Vortex shedding in shear flow past tandem square cylinders in the vicinity of a plane wall, J. Fluid Struct. 24 (3) (2008) 400–417.
[37] A. Okajima, Strouhal numbers of rectangular cylinders, J. Fluid Mech. 123 (1982) 379–398.
[38] C. Norberg, Flow around rectangular cylinders: pressure forces and wake frequencies, J. Wind Eng. Ind. Aerod. 49 (1–3) (1993) 187–196.
[39] R. Davis, E. Moore, L. Purtell, A numerical-experimental study of confined flow around rectangular cylinders, Phys. Fluids 27 (1) (1984) 46–59, 1958-1988.
[40] R. Franke, W. Rodi, B. Schönung, Numerical calculation of laminar vortex-shedding flow past cylinders, J. Wind Eng. Ind. Aerod. 35 (1990) 237–257.
[41] A.K. Sahu, R. Chhabra, V. Eswaran, Effects of Reynolds and Prandtl numbers on heat transfer from a square cylinder in the unsteady flow regime, Int. J. Heat Mass Tran. 52 (3–4) (2009) 839–850.
[42] A. Saha, G. Biswas, K. Muralidhar, Three-dimensional study of flow past a square cylinder at low Reynolds numbers, Int. J. Heat Fluid Flow 24 (1) (2003) 54–66.